Geophysical Research Letters®

Key Points:

- We conducted synchrotron X-ray diffraction measurements of a pyrolitic mantle material up to 4480 K at 122–166 GPa in a laser-heated diamond anvil cell
- Phase transition between bridgmanite and post-perovskite occurs in pyrolite within the lowermost mantle pressure range even at >4000 K
- Ubiquitous occurrence of post-perovskite above the core-mantle boundary is consistent with recent high-quality seismological observations of D" reflections

Correspondence to:

K. Hirose,
kei@elsi.jp

AGU ADVANCING EARTH AND SPACE SCIENCE

Post-Perovskite Phase Transition in the Pyrolitic Lowermost Mantle: Implications for Ubiquitous Occurrence of Post-Perovskite Above CMB

Yasuhiro Kuwayama[1], Kei Hirose[1,2] [ORCID]**, Laura Cobden[3]** [ORCID]**, Mayu Kusakabe[1], Shigehiko Tateno[2]** [ORCID]**, and Yasuo Ohishi[4]**

[1]Department of Earth and Planetary Science, The University of Tokyo, Tokyo, Japan, [2]Earth-Life Science Institute, Tokyo Institute of Technology, Tokyo, Japan, [3]Department of Earth Sciences, Utrecht University, Utrecht, The Netherlands, [4]Japan Synchrotron Radiation Research Institute, Hyogo, Japan

Abstract We conducted in situ high-pressure and -temperature X-ray diffraction measurements of a pyrolitic mantle material up to 4480 K at 122–166 GPa in a laser-heated diamond anvil cell. Results demonstrate that the phase transition between bridgmanite and post-perovskite occurs in pyrolite within the lowermost mantle pressure range even at >4000 K. It suggests the ubiquitous occurrence of post-perovskite above the core-mantle boundary, which may be consistent with recent high-quality seismology data that non-observations of D" reflections are exceptions. Combining with earlier experiments performed at and below the normal lower-mantle geotherm, our data show that the bridgmanite + post-perovskite two-phase region is ∼5 GPa thick and the dP/dT slope of the boundary is +6.5 ± 2.2 MPa/K, slightly smaller than previous theoretical calculations in MgSiO$_3$. The global presence of rheologically weak post-perovskite at the bottom of the mantle has profound implications in seismology, geodynamics, and heat transfer from the core.

Plain Language Summary (Al, Fe)-bearing MgSiO$_3$ bridgmanite is a predominant mineral in the lower mantle. While bridgmanite with the MgSiO$_3$ end-member composition is known to undergo a phase transition to post-perovskite at lowermost mantle pressures, the pressure, and thickness of the phase boundary in a typical mantle material (pyrolite) have been controversial. The present synchrotron X-ray diffraction measurements of pyrolite performed up to 4480 K around the core-mantle boundary (CMB) pressure show that the bridgmanite/post-perovskite phase transition takes place within the lowermost mantle pressure range even under high temperatures of the CMB region. The bridgmanite + post-perovskite two-phase region is found to be about 90 km thick. These results suggest the global presence of post-perovskite above the CMB, which is consistent with recent seismological observations of D" reflectors not only in the circum-Pacific high velocity regions but also in many areas away from subduction zones. Post-perovskite is rheologically weak, and its ubiquitous occurrence in the lowermost mantle has important seismological and geodynamical implications. The large positive dP/dT slope (+6.5 ± 2.2 MPa/K) of the boundary suggests that a phase transition from post-perovskite to bridgmanite assists upwelling of plumes from hot regions above the CMB.

1. Introduction

Both experiments and theory have shown that a phase transition between bridgmanite (perovskite-type structure) and post-perovskite occurs in the MgSiO$_3$ end-member under the lowermost mantle conditions (∼120 GPa and ∼2400 K) (Murakami et al., 2004; Oganov & Ono, 2004; Tateno et al., 2009), where the D" seismic velocity discontinuity is observed (e.g., Chaloner et al., 2009; D. Sun et al., 2006; He & Wen, 2011; Lay & Helmberger, 1983; Russell et al., 2001; Thomas, Garnero, & Lay, 2004; Thomas & Laske, 2015; Weber et al., 1996; Wysession et al., 1998). The pressure and sharpness of the post-perovskite phase transition have been examined also in a pyrolitic mantle material. In such a natural mantle composition, Al and Fe impurities (e.g., Catalli et al., 2009; Hirose, Takafuji, et al., 2008; Mao et al., 2005; Sinmyo et al., 2011; Tateno et al., 2005) affect the pressure and width of the transition (see a review by Hirose et al., 2015). It has been repeatedly reported that the post-perovskite phase transition occurs in a pyrolitic lowermost mantle around 120 GPa, comparable to the case in pure MgSiO$_3$, with a ∼5 GPa pressure interval (Murakami et al., 2005; Ono & Oganov, 2005; Ohta et al., 2008). On the other hand, the similar X-ray diffraction (XRD) study by Grocholski et al. (2012) found a higher transition pressure beyond the pressure range of the Earth's mantle and a much broader pressure interval of 140–168 GPa at

2500 K. In these previous experimental studies on pyrolite, however, the stabilities of bridgmanite and post-perovskite have been explored only up to 2700 K under the lowermost mantle conditions.

There are more observations of the D" seismic discontinuity in seismically fast regions associated with paleo-subduction than in slow regions, although this may be influenced by favorable earthquake source and receiver combinations. In some locations the D" discontinuity is not observed at all (see reviews by Jackson & Thomas, 2021; L. Cobden et al., 2015, and Wysession et al., 1998). A large positive dP/dT slope of the bridgmanite to post-perovskite phase transition boundary, combined with a relatively high and globally even temperature of the outermost core, might imply that bridgmanite is stable (post-perovskite is absent) to the core-mantle boundary (CMB) in relatively hot areas. In cold regions, "paired" discontinuities (positive S-wave velocity jump at the D" discontinuity and negative one at a deeper level near the CMB) might indicate the presence of bridgmanite above the CMB, instead of post-perovskite, as a consequence of back transformation from post-perovskite to bridgmanite at high temperatures in a thermal boundary layer (a double-crossing scenario; Hernlund et al., 2005; Thomas, Garnero, & Lay, 2004; Thomas, Kendall, & Lowman, 2004; Wookey et al., 2005). It is of great importance to verify these scenarios by phase equilibria experiments on multiphase assemblages that are representative of average mantle material under high temperatures of the CMB region. In addition, the Clapeyron slope of the bridgmanite/post-perovskite boundary was determined in $MgSiO_3$ end-member to be +8–10 MPa/K by theories (Oganov & Ono, 2004; Tsuchiya et al., 2004) and +5–13 MPa/K by experiments (Hirose et al., 2006; Ono & Oganov, 2005; Tateno et al., 2009). It is several times larger in magnitude than those of major upper mantle phase transitions, suggesting that the post-perovskite transition has important dynamical consequences (Nakagawa & Tackley, 2004; Tackley et al., 2007). A large positive dP/dT slope was also reported for pyrolite, but it was constrained by experiments performed in narrow temperature ranges less than ~1000 K (Grocholski et al., 2012; Ono & Oganov, 2005; Ohta et al., 2008).

In this study, we performed synchrotron XRD measurements of a pyrolitic mantle material to investigate the post-perovskite phase transition at high temperatures (3570 K and higher) including those above its solidus temperature. The results show that bridgmanite/post-perovskite phase transition occurs within the lowermost pressure range even at >4000 K. Combining with the earlier experimental results by Ohta et al. (2008), the post-perovskite-in and bridgmanite-out curves are constrained by data obtained in a wide temperature range from 1780 to 4480 K, and the dP/dT slope is found to be +6.5 ± 2.2 MPa/K when the gold pressure scale proposed by Fei et al. (2007) is applied. These results suggest that post-perovskite is present globally above the CMB, which may be consistent with recent high-quality seismological data that non-observations of D" reflection are exceptional (Jackson & Thomas, 2021).

2. Experimental Methods

High P-T experiments were performed with in situ XRD measurements in a laser-heated diamond anvil cell (DAC). We employed a symmetric-type DAC with beveled 90-μm culet diamond anvils. A starting material was the same as that used in Ohta et al. (2008); it was prepared from gel with the chemical composition of a natural peridotite KLB-1 (44.8% SiO_2, 0.2% TiO_2, 3.6% Al_2O_3, 8.2% FeO, 39.5% MgO, 3.4% CaO, and 0.3% Na_2O by weight; Takahashi, 1986), similar to pyrolite. The sample was mixed with fine gold powder and loaded into a hole at the center of a pre-indented rhenium gasket. Argon was cryogenically loaded and used as a thermal insulator.

After compression, heating was performed from both sides of the sample using a couple of 100 W single-mode Yb fiber lasers (SPI Lasers Co. Ltd.) with beam shaping optics that converts a beam with a Gaussian intensity distribution to one with a flattop distribution. The laser spot size was approximately 30 μm across. Heating duration was 3 s. A one-dimensional radial temperature profile across a hot spot was obtained by a spectro-radiometric method (e.g., Tateno, Hirose, Sinmyo, et al., 2018; Figure 1). In runs #1–3 in which the sample was partially molten, temperature shown in Table 1 corresponds to that at the boundary between a melt pool and a solid layer, which was determined by a combination of the temperature profile and a melting texture found in a cross section of a recovered sample (e.g., Hasegawa et al., 2021). For subsolidus experiments (runs #4 and #5), sample temperatures are the average in a 6 μm region at the hot spot, from which XRD data were collected. The overall temperature uncertainty may be ±5% according to Mori et al. (2017). The sample was heated only once in each run. Pressure at high temperature was determined based on the unit cell volume of gold (Fei et al., 2007). Those in the earlier experiments performed by Ohta et al. (2008) were based on the equation of state (EoS) of gold proposed
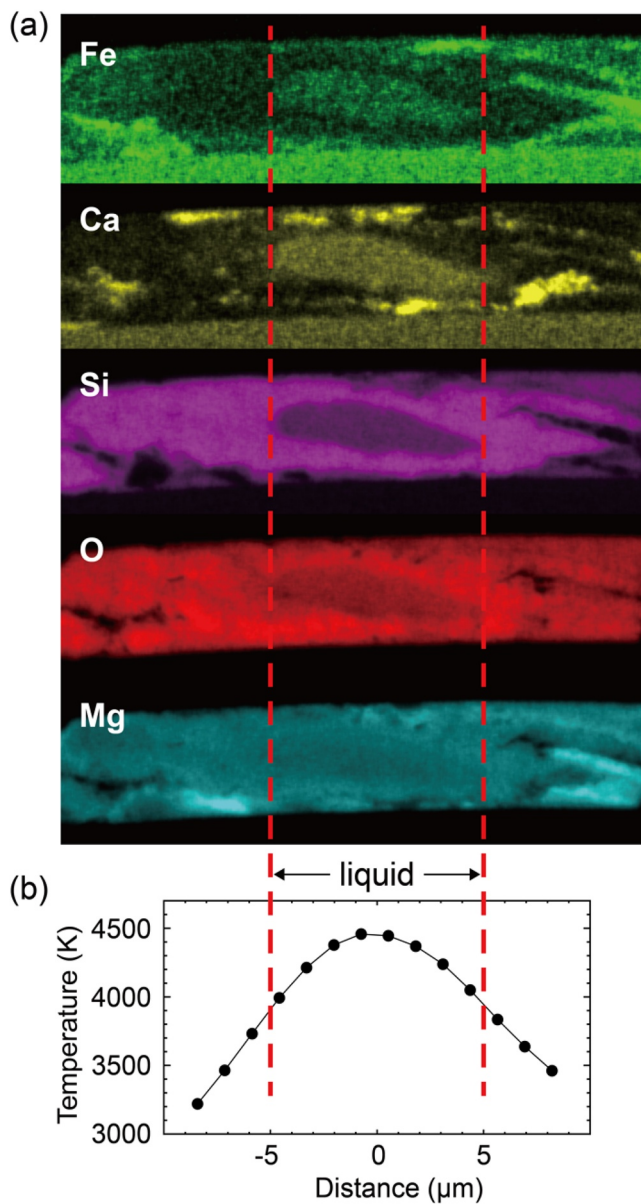
Figure 1. (a) X-ray elemental maps of the sample cross section recovered from run #1 at 122 GPa and 3910 K. (b) A corresponding temperature profile across the hot spot.

by Hirose, Sata, et al. (2008), which is not applicable at high temperatures like ~4000 K. Therefore, we recalculated the pressures in Ohta et al. (2008) using the Mie-Grüneisen-Debye EoS of gold proposed by Fei et al. (2007), in order to compare their results with those obtained in this study (Table 1).

Angle-dispersive XRD patterns were collected in situ at high *P-T* at the beamline BL10XU, SPring-8 synchrotron radiation facility (Hirao et al., 2020; Figure 2). A monochromatic incident X-ray beam was focused by stacked compound refractive lenses and collimated to approximately 6 μm area (full width at half maximum) on a sample. The wavelength was 0.4133–0.4158 Å (~30 keV). XRD data were obtained continuously during heating on a digital flat panel X-ray detector (Perkin Elmer) with exposure time of 1 s. To obtain conventional 1D diffraction patterns, 2D XRD images were integrated as a function of the 2θ angle (Seto et al., 2010).

After high *P-T* experiments, samples in runs #1–3 were recovered from the DAC, and their cross sections across the center of a laser-heated spot were prepared parallel to the compression axis by using an FIB instrument with a focused Ga ion beam (FEI, Versa3D DualBeam). X-ray elemental maps were obtained with an energy-dispersive X-ray spectrometer (EDS) attached with a field-emission-type scanning electron microscope in the dual beam FIB system (Figure 1).

3. Results

We have conducted five separate high *P-T* experiments on pyrolitic mantle material up to 156 GPa and 3570 K (Table 1). In order to avoid kinetic hindering of phase transformation especially in such a multi-component system, heating was made on an amorphous starting material at a single *P-T* condition in each run. In run #1, the sample was compressed and then heated to 3910 K at 122 GPa, higher than the solidus temperature of pyrolite (Kim et al., 2020; Nomura et al., 2014) (Figure 3a). The XRD spectrum collected in situ during heating shows that bridgmanite and minor post-perovskite, in addition to ferropericlase and davemaoite ($CaSiO_3$ perovskite), grew from the amorphous sample (Figure 2a). Microprobe analyses of the cross section of this sample, recovered from high pressure, demonstrate that there is a round pocket of quenched melt at the center, being enriched in Fe and Ca, and depleted in Si (Figure 1). This melt pocket is surrounded by a Si-rich and (Fe, Ca)-poor layer, which should represent bridgmanite (±post-perovskite) observed in the high *P-T* XRD pattern. It indicates that bridgmanite is the liquidus phase, consistent with the earlier melting experiments on pyrolite performed by Tateno et al. (2014).

Similar experiments were made in runs #2 and #3 at conditions slightly higher in both *P* and *T* (Figure 3a). Diffuse scattering signals from melt are recognized in their in situ XRD patterns (Fiquet et al., 2010), in particular for run #2 (Figure 2b). The XRD data indicate that melt coexisted with bridgmanite and minor ferropericlase (post-perovskite is absent) in run #2 at 128 GPa and 4480 K. In contrast, the high *P-T* XRD pattern is dominated by post-perovskite in run #3 performed at 130 GPa and 4300 K (Figure 2c). In addition, runs #4 and #5 were conducted at 156–166 GPa and 3570–3860 K under subsolidus conditions (Figure 3a), which is supported by observations that the number of peaks and their relative intensities in XRD patterns did not change upon quenching temperature. The present above-solidus and subsolidus experiments support the relatively low solidus temperature of pyrolite at the CMB pressure (Kim et al., 2020; Nomura et al., 2014).

These results of runs #1–3 constrain the post-perovskite-in and bridgmanite-out conditions around 4000 K (Figure 3a). While partial melts coexisted with both bridgmanite and post-perovskite in runs #1 and 3, only one of

Table 1
Experimental Results

Run#	Volume of Au (Å³)	Pressure (GPa)	Temperature (K)	Phase assemblage
This study				
#1	52.19(5)	121.9(2)	3910	Bdg + PPv (trace) + Fp + CaPv + melt
#2	52.06(12)	128.1(3)	4480	Bdg + Fp + melt
#3	51.82(4)	129.6(2)	4300	PPv + Bdg (trace) + melt
#4	49.08(8)	165.9(3)	3860	PPv + Fp + CaPv
#5	49.53(8)	156.1(3)	3570	PPv + Fp + CaPv
Ohta et al. (2008)				
#1–1	51.91(11)	108.2(3)	1780	Bdg + Fp + CaPv
#1–2	51.93(7)	109.4(2)	1960	Bdg + Fp + CaPv
#1–3	52.26(12)	110.0(3)	2540	Bdg + Fp + CaPv
#2–1	51.70(8)	110.9(2)	1800	Bdg + PPv (trace) + Fp + CaPv
#2–2	51.75(9)	111.6(3)	1950	Bdg + PPv (trace) + Fp + CaPv
#3	51.43(6)	115.6(2)	1940	PPv + Bdg + Fp + CaPv
#4	53.43(3)	95.0(2)	2300	Bdg + Fp + CaPv
#5	52.33(17)	105.4(3)	2070	Bdg + Fp + CaPv
#6	51.56(1)	118.8(2)	2550	PPv + Fp + CaPv
#7	50.79(14)	126.6(4)	2250	PPv + Fp + CaPv
#8	50.72(20)	129.1(4)	2450	PPv + Fp + CaPv

Note. The numbers in parentheses represent one standard deviation in the last digits. Bdg, bridgmanite; PPv, post-perovskite; Fp, ferropericlase; CaPv, CaSiO$_3$ perovskite.

them was dominant in each of these experiments (Figures 2a and 2c), indicating that their *P-T* conditions should be close to the post-perovskite-in and bridgmanite-out curves, respectively. The width of the post-perovskite phase transition should thus be about 5 GPa, corresponding to a lowermost mantle depth range of 90 km, similar to that observed by Ohta et al. (2008) at lower temperatures below 2550 K. When combined with Ohta et al. (2008)'s data (Table 1), our results obtained in a wide temperature range from 1780 to 4480 K at 108–130 GPa show the d*P*/d*T* slope of these post-perovskite-in and bridgmanite-out curves to be +6.5 ± 2.2 MPa/K when assuming that the slope does not change above the solidus curve (Figure 3a). Indeed, upon partial melting both bridgmanite and post-perovskite become depleted in iron and in aluminum to a small extent (D. Andrault et al., 2012; Tateno et al., 2014), which would affect the phase transition boundary (e.g., D. Andrault et al., 2010; N. Sun et al., 2018; Sinmyo et al., 2011; Wang et al., 2019). Nevertheless, the effect of such compositional change above solidus temperature is not clear in the present experiments (Figure 3a).

4. Discussion

4.1. Post-Perovskite Phase Transition in Pyrolitic Lowermost Mantle

The pressure (~120 GPa at 2400 K) of the post-perovskite phase transition we obtained for pyrolite along the normal lower-mantle geotherm (Brown & Shankland, 1981) is in agreement with the depth of the D" seismic discontinuity (see Wysession et al., 1998 and L. Cobden et al., 2015 for reviews). While earlier XRD measurements have also repeatedly demonstrated that it takes place in pyrolite around 120 GPa (Murakami et al., 2005; Ono & Oganov, 2005; Ohta et al., 2008), the experiments carried out by Grocholski et al. (2012) found the phase transition at 140–168 GPa and 2500 K. Such a large discrepancy is not reconciled with the difference in pressure scale employed to determine experimental pressures (Figure 3b), although pressure estimates can change as much as 15 GPa in the relevant pressure range (see a review by Hirose et al., 2015). The difference in a pressure medium is also unlikely to be an important source of the discrepancy; noble gas (argon or neon) pressure medium was used in Ono and Oganov (2005) and this study as well as in Grocholski et al. (2012).
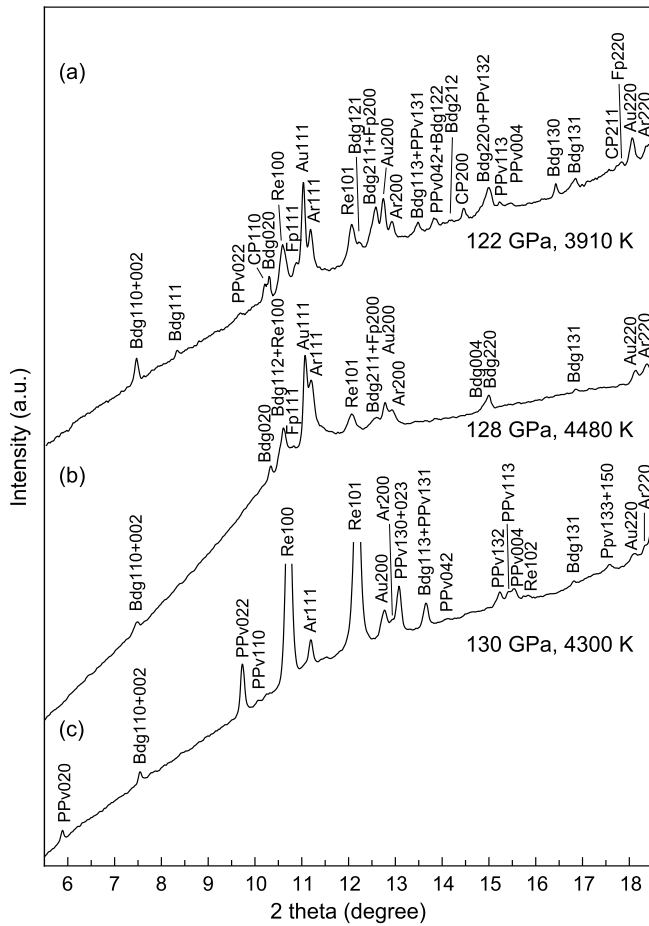
Figure 2. X-ray diffraction patterns at (a) 122 GPa and 3910 K, (b) 128 GPa and 4480 K, and (c) 130 GPa and 4300 K. Bdg, MgSiO$_3$-rich perovskite; PPv, post-perovskite; Fp, ferropericlase; CP, CaSiO$_3$ perovskite; Au, gold; Ar, argon pressure medium; Re, rhenium gasket.

The dP/dT slope of the transition boundary (+6.5 ± 2.2 MPa/K) found in the present experiments for pyrolite is slightly smaller than that reported by earlier ab initio calculations for MgSiO$_3$ (+7.5–9.6 MPa/K) (Oganov & Ono, 2004; Tsuchiya et al., 2004). Experimental determination of the dP/dT slope depends on the choice of the pressure scale used to calculate pressures. When different EoSs of gold (Anderson et al., 1989; Jamieson et al., 1982; Shim et al., 2002; Tsuchiya, 2003) other than the Fei et al. (2007)'s EoS are employed, the slope becomes smaller ranging from +3 to +7 MPa/K (Figure 3b). The pressure range of the transition also becomes lower. While Hirose et al. (2006) reported the slope of +4.7 MPa/K for pure MgSiO$_3$ based on the Tsuchiya (2003)'s Au scale, it is recalculated to be +7.1 MPa/K with the Fei's scale, which is similar to the slope obtained for pyrolite in this study. The dP/dT slope depends also on the internal pressure standard (Hirose et al., 2015). Based on a comparison between pressures estimated by the EoSs of Au and MgO at high temperatures in Hirose et al. (2006), the post-perovskite-in and bridgmanite-out boundaries in pyrolite are estimated on the basis of the MgO pressure scale (Speziale et al., 2001) in Figure 3b. They exhibit the slope of +11.1 MPa/K, comparable to +13 MPa/K in MgSiO$_3$ found by Tateno et al. (2009) using the Speziale's MgO scale.

The present experiments and the earlier ones by Ohta et al. (2008) demonstrate that bridgmanite and post-perovskite coexist in a pyrolitic mantle material in a ~5 GPa pressure interval at ~4000 K and ~2000–2500 K, respectively (Figure 3a). It is comparable to recent theoretical calculations of the thickness of the bridgmanite + post-perovskite two-phase region at 2500 K; 0.6, 1.9, and 12.5 GPa in MgSiO$_3$ containing 10 mol% Fe^{2+}SiO$_3$, 5 mol% Al$_2$O$_3$, and 5 mol% Fe^{3+}AlO$_3$, respectively (Wang et al., 2019), while previous experimental studies reported much wider thickness, more than 20 GPa in (Al, Fe)-bearing MgSiO$_3$ (Catalli et al., 2009; D. Andrault et al., 2010; N. Sun et al., 2018).

4.2. Ubiquitous Occurrence of Post-Perovskite Above CMB

These results show that post-perovskite transforms into bridgmanite above 4800 K at the CMB (Figure 3a). It is much higher than the present-day CMB temperature, with estimates ranging from 3600 to 4300 K (e.g., Kim et al., 2020; Lay et al., 2008; Nomura et al., 2014). If the deep lower mantle is dominated by a pyrolitic material, it suggests that a) the bridgmanite/post-perovskite phase transition takes place globally in the lowermost mantle although the transition is not sharp, and b) post-perovskite is present ubiquitously above the CMB. These conclusions do not depend on the choice of the EoS of gold to determine experimental pressures (Figure 3b). If the MgO pressure scale is employed, we obtain a larger dP/dT slope of the transition boundary and a wider stability field of bridgmanite at relatively high temperatures. Even in this case, post-perovskite is stable (bridgmanite does not appear) at the bottom of the mantle as far as the CMB temperature is less than 3550 K (Figure 3b). Since the lowermost mantle is not globally molten, such relatively low CMB temperature is supported by recent determinations of the solidus temperature of pyrolite at 135 GPa; 3570 ± 200 K by Nomura et al. (2014) and 3430 ± 130 K by Kim et al. (2020).

The ~5 GPa pressure width of the bridgmanite + post-perovskite coexistence corresponds to ~90 km depth interval in the lowermost mantle. The sharpness of the D" seismic discontinuity should be less than this (Weber et al., 1996) and potentially as narrow as 8–30 km (i.e., <2 GPa) (Lay, 2008; Lay & Young, 1989; Wysession et al., 1998), suggesting that the bridgmanite/post-perovskite transition boundary in pyrolite may not be observed as a seismic velocity discontinuity, as argued by Lay (2008).

The D" discontinuity is found mainly in high-velocity regions underneath the circum-Pacific (Jackson & Thomas, 2021; L. Cobden et al., 2015; Wysession et al., 1998), and this has been attributed to the enrichment in subducted depleted mantle materials (harzburgitic rocks), in which the bridgmanite to post-perovskite phase
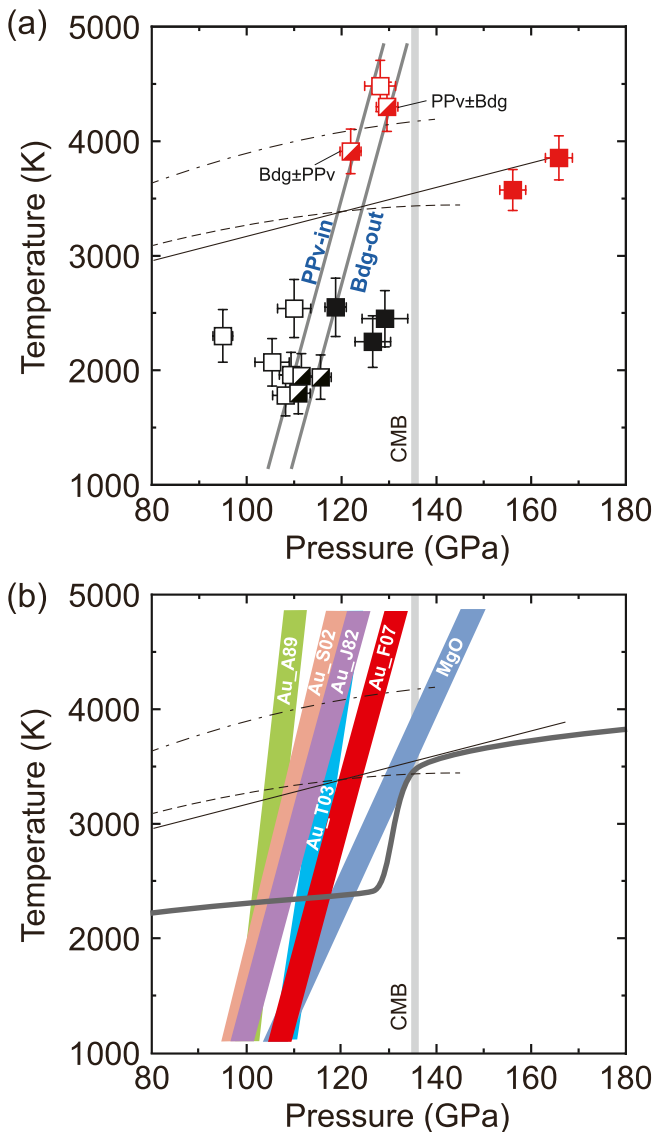
Figure 3. (a) Phase boundary between bridgmanite (Bdg) and post-perovskite (PPv). Open and solid symbols represent the stabilities of bridgmanite and post-perovskite, respectively. Half-filled symbols show the coexistence of both phases. Red symbols, this study; black symbols, from Ohta et al. (2008). Thin solid, broken, and dashed-dotted curves indicate solidus temperatures of pyrolite reported by Nomura et al. (2014), Kim et al. (2020), and Fiquet et al. (2010), respectively. (b) Changes in the phase boundary by using different equation of state of gold (Anderson et al., 1989; Fei et al., 2007; Jamieson et al., 1982; Shim et al., 2002; Tsuchiya, 2003) and MgO (Speziale et al., 2001) to calculate experimental pressures. Gray bold curve shows the normal geotherm (Brown & Shankland, 1981) considering the core-mantle boundary temperature is less than the solidus curve of pyrolite.

transition occurs in a narrow pressure range because they are poor in Al and Fe impurities (Grocholski et al., 2012). D" seismic reflections could also be produced in these regions by scattering off chemical heterogeneities (e.g., Cobden & Thomas, 2013). On the other hand, there are observations of the D" discontinuity beneath the central Pacific as well (Cobden & Thomas, 2013; Jackson & Thomas, 2021; Lay et al., 2006). Post-perovskite should be predominant above the CMB including such areas away from the circum-Pacific high-velocity regions. Our results do not preclude the bridgmanite/post-perovskite transition in pyrolite from generating D" reflections; stress-induced re-equilibration within the two-phase region can produce high amplitude seismic reflections, even when the transition region is thick (Langrand et al., 2019). Additionally, development of the lattice-preferred orientation of post-perovskite may generate sharp reflectors within a broad two-phase region (Ammann et al., 2010; Pisconti et al., 2019).

Indeed, the ubiquitous occurrence of post-perovskite above the CMB has been supported by statistical analyses of seismic observations (L. Cobden et al., 2012, 2015) and by comparisons between seismic tomography and geodynamic models (Koelemeijer et al., 2018). Mineral physics models with post-perovskite are compatible with both global and local seismic data of *S*- and *P*-wave velocity perturbations in the lowermost mantle rather than post-perovskite-free models. Recent high-quality seismological data indicate that non-observations of a discontinuity in the lowermost mantle are not common but exceptional (Jackson & Thomas, 2021).

The ubiquitous presence of post-perovskite above the CMB has profound geodynamical consequences. Because of its proximity to the CMB, the global occurrence of the bridgmanite/post-perovskite phase transition with the large positive d*P*/d*T* slope (+6.5 ± 2.2 MPa/K) destabilizes the thermal boundary layer developed at the bottom of the mantle and enhances plume upwelling (Hirose et al., 2015; Li et al., 2014; Nakagawa & Tackley, 2004). Theoretical calculations and experiments demonstrated that post-perovskite is at least five times weaker than bridgmanite (Ammann et al., 2010; Hunt et al., 2009). The low-viscosity D" layer allows cold slab materials to spread extensively above the CMB, leading to an increase in heat transfer from the core (Buffett, 2007; Cizkova et al., 2010). It also enhances the segregation of MORB crust materials from the rest of the subducted slab, contributing to the formation of dense piles above the CMB (Nakagawa & Tackley, 2011).

Ultralow-velocity zones are observed locally above the CMB, likely representing partially molten materials with relatively low melting temperatures such as FeO-rich ones (Boukaré et al., 2015; Helffrich et al., 2020). On the other hand, when the CMB temperature was higher in the past (Labrosse, 2015), the lowermost mantle could have been globally molten. The present experiments demonstrate that post-perovskite is the liquidus phase (the first phase to appear upon crystallization) in a pyrolitic lowermost mantle when we employ the Au pressure scale (Figure 3). The behavior of trace elements during partial melting involving post-perovskite may be different from that with bridgmanite; water and Na_2O have been shown to be partitioned more into Al-bearing post-perovskite than into bridgmanite (Hirose et al., 2005; Tateno, Hirose, Sakata, et al., 2018, Townsend et al., 2016). Partitioning of trace elements between melt and post-perovskite is yet to be explored.

5. Conclusions

We have examined the phase transition between bridgmanite and post-perovskite in a pyrolitic mantle material at high temperatures (3570–4480 K) around the CMB pressure. The results demonstrate that it occurs in pyrolite within the lowermost mantle pressure range even at >4000 K. They also indicate the two-phase coexisting region of ~5 GPa and a dP/dT slope of $+6.5 \pm 2.2$ MPa/K, when combined with earlier experimental results obtained at lower temperatures (Ohta et al., 2008).

The global presence of post-perovskite above the CMB is consistent with recent high-quality seismological observations of the D" seismic reflections; they are found not only in the circum-Pacific high-velocity regions but also in many places away from such (presumably) cold areas (Jackson & Thomas, 2021). The 5 GPa two-phase coexisting interval may be too thick for the bridgmanite/post-perovskite phase transition in pyrolite to be the cause of seismic reflections. Alternatively the seismic discontinuity observed underneath subduction zones could be attributed to the post-perovskite phase transition in depleted peridotite materials that should be abundant in such areas (Grocholski et al., 2012) or caused by scattering off chemical heterogeneities that derive from subductions of former oceanic plates (Cobden & Thomas, 2013). The D" reflections observed in areas distant from subduction zones can be formed by other mechanisms such as deformation of weak post-perovskite within a two-phase region (Ammann et al., 2010; Pisconti et al., 2019). Indeed, the ubiquitous occurrence of post-perovskite above the CMB is supported by a statistical interpretation of seismic observations (L. Cobden et al., 2012, 2015) and by comparisons of seismic tomographies between observed and synthesized from geodynamic simulations (Koelemeijer et al., 2018). The global presence of rheologically weak post-perovskite at the bottom of the mantle has profound implications for the dynamics and thermal histories of both the mantle and the core.

Data Availability Statement

Datasets for this research are found in Table 1 available online (from https://doi.org/10.5281/zenodo.5513281).

References

Ammann, M. W., Brodholt, J. P., Wookey, J., & Dobson, D. P. (2010). First-principles constraints on diffusion in lower-mantle minerals and a weak D" layer. *Nature*, *465*, 462–465. https://doi.org/10.1038/nature09052

Anderson, O. L., Isaak, D. G., & Yamamoto, S. (1989). Anharmonicity and the equation of state for gold. *Journal of Applied Physics*, *65*, 1534–1543. https://doi.org/10.1063/1.342969

Andrault, D., Muñoz, M., Bolfan-Casanova, N., Guignot, N., Perrillat, J.-P., Aquilanti, G., & Pascarelli, S. (2010). Experimental evidence for perovskite and post-perovskite coexistence throughout the whole D" region. *Earth and Planetary Science Letters*, *293*, 90–96. https://doi.org/10.1016/j.epsl.2010.02.026

Andrault, D., Petitgirard, S., Lo Nigro, G., Devidal, J. L., Veronesi, G., Garbarino, G., & Mezouar, M. (2012). Solid-liquid iron partitioning in Earth's deep mantle. *Nature*, *487*, 354–357. https://doi.org/10.1038/nature11294

Boukaré, C.-E., Ricard, Y., & Fiquet, G. (2015). Thermodynamics of the MgO-FeO-SiO$_2$ system up to 140 GPa: Application to the crystallization of Earth's magma ocean. *Journal of Geophysical Research: Solid Earth*, *120*, 6085–6101. https://doi.org/10.1002/2015JB011929

Brown, M. J., & Shankland, T. J. (1981). Thermodynamic parameters in the Earth as determined from seismic profiles. *Geophysical Journal of the Royal Astronomical Society*, *66*, 579–596. https://doi.org/10.1111/j.1365-246x.1981.tb04891.x

Buffett, B. A. (2007). A bound on heat flow below a double crossing of the perovskite-postperovskite phase transition. *Geophysical Research Letters*, *34*, L17302. https://doi.org/10.1029/2007GL030930

Catalli, K., Shim, S. H., & Prakapenka, V. (2009). Thickness and Clapeyron slope of the post-perovskite boundary. *Nature*, *462*, 782–785. https://doi.org/10.1038/nature08598

Chaloner, J. W., Thomas, C., & Rietbrock, A. (2009). *P*- and *S*-wave reflectors in D" beneath southeast Asia. *Geophysical Journal International*, *179*, 1080–1092. https://doi.org/10.1111/j.1365-246X.2009.04328.x

Cizkova, H., Cadek, O., Matyska, C., & Yuen, D. A. (2010). Implications of post-perovskite transport properties for core–mantle dynamics. *Physics of the Earth and Planetary Interiors*, *180*, 235–243. https://doi.org/10.1016/j.pepi.2009.08.008

Cobden, L., & Thomas, C. (2013). The origin of D" reflections: A systematic study of seismic array data sets. *Geophysical Journal International*, *194*, 1091–1118. https://doi.org/10.1093/gji/ggt152

Cobden, L., Mosca, I., Trampert, J., & Ritsema, J. (2012). On the likelihood of post-perovskite near the core-mantle boundary: A statistical interpretation of seismic observations. *Physics of the Earth and Planetary Interiors*, *210–211*, 21–35. https://doi.org/10.1016/j.pepi.2012.08.007

Cobden, L., Thomas, C., & Trampert, J. (2015). Seismic detection of post-perovskite inside the Earth. In A. Khan, & F. Deschamps (Eds.), *The Earth's heterogeneous mantle* (pp. 391–440). Switzerland: Springer Geophysics. https://doi.org/10.1007/978-3-319-15627-9_13

Fei, Y., Ricolleau, A., Frank, M., Mibe, K., Shen, G., & Prakapenka, V. (2007). Toward an internally consistent pressure scale. *Proceedings of the National Academy of Sciences of the United States of America*, *104*, 9182–9186. https://doi.org/10.1073/pnas.0609013104

Fiquet, G., Auzende, A. L., Siebert, J., Corgne, A., Bureau, H., Ozawa, H., & Garbarino, G. (2010). Melting of peridotite to 140 gigapascals. *Science*, *329*, 1516–1518. https://doi.org/10.1126/science.1192448

Grocholski, B., Catalli, K., Shim, S. H., & Prakapenka, V. (2012). Mineralogical effects on the detectability of the postperovskite boundary. *Proceedings of the National Academy of Sciences of the United States of America*, *109*, 2275–2279. https://doi.org/10.1073/pnas.1109204109

Hasegawa, M., Hirose, K., Oka, K., & Ohishi, Y. (2021). Liquidus phase relations and solid-liquid partitioning in the Fe-Si-C system under core pressures. *Geophysical Research Letters*, *48*, e2021GL092681. https://doi.org/10.1029/2021GL092681

He, Y. M., & Wen, L. X. (2011). Seismic velocity structures and detailed features of the D″ discontinuity near the core-mantle boundary beneath eastern Eurasia. *Physics of the Earth and Planetary Interiors*, *189*, 176–184. https://doi.org/10.1016/j.pepi.2011.09.002

Helffrich, G., Hirose, K., & Nomura, R. (2020). Thermodynamical modeling of liquid Fe-Si-Mg-O: Molten magnesium silicate release from the core. *Geophysical Research Letters*, *47*, e2020GL089218. https://doi.org/10.1029/2020GL089218

Hernlund, J. W., Thomas, C., & Tackley, P. J. (2005). A doubling of the postperovskite phase boundary and structure of the Earth's lower mantle. *Nature*, *434*, 882–886. https://doi.org/10.1038/nature03472

Hirao, N., Kawaguchi, S., Hirose, K., Shimizu, K., Ohtani, E., & Ohishi, Y. (2020). New developments in high-pressure X-ray diffraction beamline for diamond anvil cell at SPring-8. *Matter and Radiation at Extremes*, *5*, 018403. https://doi.org/10.1063/1.5126038

Hirose, K., Sata, N., Komabayashi, T., & Ohishi, Y. (2008). Simultaneous volume measurements of Au and MgO to 140 GPa and thermal equation of state of Au based on MgO pressure scale. *Physics of the Earth and Planetary Interiors*, *167*, 149–154. https://doi.org/10.1016/j.pepi.2008.03.002

Hirose, K., Sinmyo, R., Sata, N., & Ohishi, Y. (2006). Determination of post-perovskite phase transition boundary in $MgSiO_3$ using Au and MgO internal pressure standards. *Geophysical Research Letters*, *33*, L01310. https://doi.org/10.1029/2005GL024468

Hirose, K., Takafuji, N., Fujino, K., Shieh, S. R., & Duffy, T. S. (2008). Iron partitioning between perovskite and post-perovskite: A transmission electron microscope study. *American Mineralogist*, *93*, 1678–1681. https://doi.org/10.2138/am.2008.3001

Hirose, K., Takafuji, N., Sata, N., & Ohishi, Y. (2005). Phase transition and density of subducted MORB crust in the lower mantle. *Earth and Planetary Science Letters*, *237*, 239–251. https://doi.org/10.1016/j.epsl.2005.06.035

Hirose, K., Wentzcovitch, R., Yuen, D., & Lay, T. (2015). Mineralogy of the deep mantle – The post-perovskite phase and its geophysical significance. In G. Schubert (Ed.), *Treatise on geophysics* (2nd ed., Vol. 2, pp. 85–115). Elsevier. https://doi.org/10.1016/B978-0-444-53802-4.00054-3

Hunt, S. A., Weidner, D. J., Li, L., Wang, L., Walte, N. P., Brodholt, J. P., & Dobson, D. P. (2009). Weakening of calcium iridate during its transformation from perovskite to post-perovskite. *Nature Geosciences*, *2*, 794–797. https://doi.org/10.1038/NGEO663

Jackson, J. M., & Thomas, C. (2021). Seismic and mineral physics constraints on the D″ Layer. In H. Marquardt, M. Ballmer, S. Cottaar, & J. Konter (Eds.), *Mantle convection and surface expressions, Geophysical Monograph Series* (Vol. 263, pp. 193–227). John Wiley & Sons, Inc. https://doi.org/10.1002/9781119528609.ch8

Jamieson, J. C., Fritz, J. N., & Manghnani, M. H. (1982). Pressure measurement at high temperature in x-ray diffraction studies: Gold as a primary standard. In S. Akimoto, & M. H. Manghnani (Eds.), *High-pressure research in geophysics* (pp. 27–48). CAPJ. https://doi.org/10.1007/978-94-009-7867-6_3

Kim, T., Ko, B., Greenberg, E., Prakapenka, V., Shim, S. H., & Lee, Y. (2020). Low melting temperature of anhydrous mantle materials at the core-mantle boundary. *Geophysical Research Letters*, *47*, e2020GL089345. https://doi.org/10.1029/2020GL089345

Koelemeijer, P., Schuberth, B. S. A., Davies, D. R., Deuss, A., & Ritsema, J. (2018). Constraints on the presence of post-perovskite in Earth's lowermost mantle from tomographic-geodynamic model comparisons. *Earth and Planetary Science Letters*, *494*, 226–238. https://doi.org/10.1016/j.epsl.2018.04.056

Labrosse, S. (2015). Thermal evolution of the core with a high thermal conductivity. *Physics of the Earth and Planetary Interiors*, *247*, 36–55. https://doi.org/10.1016/j.pepi.2015.02.002

Langrand, C., Andrault, D., Durand, S., Konôpková, Z., Hilairet, N., Thomas, C., & Merkel, S. (2019). Kinetics and detectability of the bridgmanite to post-perovskite transformation in the Earth's D″ layer. *Nature Communications*, *10*, 5680. https://doi.org/10.1038/s41467-019-13482-x

Lay, T. (2008). Sharpness of the D″ discontinuity beneath the Cocos Plate: Implications for the perovskite to post-perovskite phase transition. *Geophysical Research Letters*, *35*, L03304. https://doi.org/10.1029/2007GL032465

Lay, T., & Helmberger, D. V. (1983). A lower mantle S-wave triplication and the shear velocity structure of D. *Geophysical Journal International*, *75*, 799–837. https://doi.org/10.1111/j.1365-246X.1983.tb05010.x

Lay, T., Hernlund, J., & Buffett, B. A. (2008). Core–mantle boundary heat flow. *Nature Geoscience*, *1*, 25–32. https://doi.org/10.1038/ngeo.2007.44

Lay, T., Hernlund, J., Garnero, E. J., & Thorne, S. (2006). A post-perovskite lens and D″ heat flux beneath the central Pacific. *Science*, *314*, 1272–1276. https://doi.org/10.1126/science.1133280

Lay, T., & Young, C. J. (1989). Waveform complexity in teleseismic broadband SH displacements: Slab diffractions or deep mantle reflections? *Geophysical Research Letters*, *16*, 605–608. https://doi.org/10.1029/gl016i007p00605

Li, Y., Deschamps, F., & Tackley, P. J. (2014). Effects of low-viscosity post-perovskite on the stability and structure of primordial reservoirs in the lower mantle. *Geophysical Research Letters*, *41*, 7089–7097. https://doi.org/10.1002/2014GL061362

Mao, W. L., Meng, Y., Shen, G., Prakapenka, V. B., Campbell, A. J., Heinz, D. L., et al. (2005). Iron-rich silicates in the Earth's D″ layer. *Proceedings of the National Academy of Sciences of the United States of America*, *102*, 9751–9753. https://doi.org/10.1073/pnas.0503737102

Mori, Y., Ozawa, H., Hirose, K., Sinmyo, R., Tateno, S., Morard, G., & Ohishi, Y. (2017). Melting experiments on Fe–Fe_3S system to 254 GPa. *Earth and Planetary Science Letters*, *464*, 135–141. https://doi.org/10.1016/j.epsl.2017.02.021

Murakami, M., Hirose, K., Kawamura, K., Sata, N., & Ohishi, Y. (2004). Post-perovskite phase transition in $MgSiO_3$. *Science*, *304*, 855–858. https://doi.org/10.1126/science.1095932

Murakami, M., Hirose, K., Sata, N., & Ohishi, Y. (2005). Post-perovskite phase transition and crystal chemistry in the pyrolitic lowermost mantle. *Geophysical Research Letters*, *32*, L03304. https://doi.org/10.1029/2004GL021956

Nakagawa, T., & Tackley, P. J. (2004). Effects of a perovskite–post perovskite phase change mantle boundary in compressible mantle. *Geophysical Research Letters*, *31*, L16611. https://doi.org/10.1029/2004GL020648

Nakagawa, T., & Tackley, P. J. (2011). Effects of low-viscosity post-perovskite on thermo- chemical mantle convection in a 3-D spherical shell. *Geophysical Research Letters*, *38*, L04309. https://doi.org/10.1029/2010GL046494

Nomura, R., Hirose, K., Uesugi, K., Ohishi, Y., Tsuchiyama, A., Miyake, A., et al. (2014). Low core-mantle boundary temperature inferred from the solidus of pyrolite. *Science*, *343*, 522–525. https://doi.org/10.1126/science.1248186

Oganov, A. R., & Ono, S. (2004). Theoretical and experimental evidence for a post- perovskite phase of $MgSiO_3$ in Earth's D″ layer. *Nature*, *430*, 445–448. https://doi.org/10.1038/nature02701

Ohta, K., Hirose, K., Lay, T., Sata, N., & Ohishi, Y. (2008). Phase transitions in pyrolite and MORB at lowermost mantle conditions: Implications for a MORB-rich pile above the core-mantle boundary. *Earth and Planetary Science Letters*, *267*, 107–117. https://doi.org/10.1016/j.epsl.2007.11.037

Ono, S., & Oganov, A. R. (2005). In situ observations of phase transition between perovskite and $CaIrO_3$-type phase in $MgSiO_3$ and pyrolitic mantle composition. *Earth and Planetary Science Letters*, *236*, 914–932. https://doi.org/10.1016/j.epsl.2005.06.001

Pisconti, A., Thomas, C., & Wookey, J. (2019). Discriminating between causes of D″ anisotropy using reflections and splitting measurements for a single path. *Journal of Geophysical Research: Solid Earth*, *124*, 4811–4830. https://doi.org/10.1029/2018jb016993

Russell, S. A., Reasoner, C., Lay, T., & Revenaugh, J. (2001). Coexisting shear- and compressional-wave seismic velocity discontinuities beneath the central Pacific. *Geophysical Research Letters*, *28*, 2281–2284. https://doi.org/10.1029/2000GL012553

Seto, Y., Nishio-Hamane, D., Nagai, T., & Sata, N. (2010). Development of a software suite on X-ray diffraction experiments. *The Review of High Pressure Science and Technology*, *20*, 269–276. https://doi.org/10.4131/jshpreview.20.269

Shim, S., Duffy, T. S., & Takemura, K. (2002). Equation of state of gold and its application to the phase boundaries near 660 km depth in the Earth's mantle. *Earth and Planetary Science Letters*, *203*, 729–739. https://doi.org/10.1016/S0012-821X(02)00917-2

Sinmyo, R., Hirose, K., Muto, S., Ohishi, Y., & Yasuhara, A. (2011). The valence state and partitioning of iron in the Earth's lowermost mantle. *Journal of Geophysical Research*, *116*, B07205. https://doi.org/10.1029/2010JB008179

Speziale, S., Zha, C., Duffy, T. S., Hemley, R. J., & Mao, H. K. (2001). Quasi-hydrostatic compression of magnesium oxide to 52 GPa: Implications for the pressure–volume–temperature equation of state. *Journal of Geophysical Research*, *106*, 515–528. https://doi.org/10.1029/2000JB900318

Sun, D., Song, T. R. A., & Helmberger, D. (2006). Complexity of D" in the presence of slab-debris and phase changes. *Geophysical Research Letters*, *33*, L12S07. https://doi.org/10.1029/2005GL025384

Sun, N., Wei, W., Han, S., Song, J., Li, X., Duan, Y., et al. (2018). Phase transition and thermal equations of state of (Fe,Al)-bridgmanite and post-perovskite: Implication for the chemical heterogeneity at the lowermost mantle. *Earth and Planetary Science Letters*, *490*, 161–169. https://doi.org/10.1016/j.epsl.2018.03.004

Tackley, P. J., Nakagawa, T., & Hernlund, J. W. (2007). Influence of the post-perovskite transition on thermal and thermo-chemical mantle convection. In K. Hirose, J. Brodholt, T. Lay, & D. Yuen (Eds.), *Post-perovskite: The last mantle phase transition, Geophysical Monograph Series* (Vol. 174, pp. 229–247). American Geophysical Union. https://doi.org/10.1029/174gm16

Takahashi, E. (1986). Melting of a dry peridotite KLB-1 up to 14 GPa: Implications on the origin of peridotite upper mantle. *Journal of Geophysical Research*, *91*, 9367–9382. https://doi.org/10.1029/JB091iB09p09367

Tateno, S., Hirose, K., & Ohishi, Y. (2014). Melting experiments on peridotite to lowermost mantle conditions. *Journal of Geophysical Research: Solid Earth*, *119*, 4684–4694. https://doi.org/10.1002/2013JB010616

Tateno, S., Hirose, K., Sakata, S., Yonemitsu, K., Ozawa, H., Hirata, T., et al. (2018). Melting phase relations and element partitioning in MORB to lowermost mantle conditions. *Journal of Geophysical Research: Solid Earth*, *123*, 5515–5531. https://doi.org/10.1029/2018JB015790

Tateno, S., Hirose, K., Sata, N., & Ohishi, Y. (2005). Phase relations in $Mg_3Al_2Si_3O_{12}$ to 180 GPa: Effect of Al on post-perovskite phase transition. *Geophysical Research Letters*, *32*, L15306. https://doi.org/10.1029/2005GL023309

Tateno, S., Hirose, K., Sata, N., & Ohishi, Y. (2009). Determination of post-perovskite phase transition boundary up to 4,400 K and implications for thermal structure in D" layer. *Earth and Planetary Science Letters*, *277*, 130–136. https://doi.org/10.1016/J.EPSL.2008.10.004

Tateno, S., Hirose, K., Sinmyo, R., Morard, G., Hirao, N., & Ohishi, Y. (2018). Melting of Fe–Si–S alloys to core pressures: Silicon in the core? *American Mineralogist*, *103*, 742–748. https://doi.org/10.2138/am-2018-6299

Thomas, C., Garnero, E. J., & Lay, T. (2004). High-resolution imaging of lowermost mantle structure under the Cocos Plate. *Journal of Geophysical Research*, *109*, B08307. https://doi.org/10.1029/2004JB003013

Thomas, C., Kendall, J. M., & Lowman, J. (2004). Lower-mantle seismic discontinuities and the thermal morphology of subducted slabs. *Earth and Planetary Science Letters*, *225*, 105–113. https://doi.org/10.1016/j.epsl.2004.05.038

Thomas, C., & Laske, G. (2015). D" observations in the Pacific from PLUME ocean bottom seismometer recordings. *Geophysical Journal International*, *200*, 851–862. https://doi.org/10.1093/gji/ggu441

Townsend, J. P., Tsuchiya, J., Bina, C. R., & Jacobsen, S. D. (2016). Water partitioning between bridgmanite and postperovskite in the lowermost mantle. *Earth and Planetary Science Letters*, *454*, 20–27. https://doi.org/10.1016/j.epsl.2016.08.009

Tsuchiya, T. (2003). First-principles prediction of the *P–V–T* equation of state of gold and the 660-km discontinuity in Earth's mantle. *Journal of Geophysical Research*, *108*, 2462. https://doi.org/10.1029/2003JB002446

Tsuchiya, T., Tsuchiya, J., Umemoto, K., & Wentzcovitch, R. M. (2004). Phase transition in $MgSiO_3$ perovskite in the Earth's lower mantle. *Earth and Planetary Science Letters*, *224*, 241–248. https://doi.org/10.1016/j.epsl.2004.05.017

Wang, X., Tsuchiya, T., & Zeng, Z. (2019). Effects of Fe and Al incorporations on the bridgmanite–postperovskite coexistence domain. *Comptes Rendus Geoscience*, *351*, 141–146. https://doi.org/10.1016/j.crte.2018.10.003

Weber, M., Davis, J. P., Thomas, C., Krüger, F., Scherbaum, F., Schlittenhardt, J., & Körnig, M. (1996). The structure of the lowermost mantle as determined from using seismic arrays. In E. Boschi, G. Ekström, & A. Morelli (Eds.), *Seismic modelling of the Earth's structure* (pp. 399–442). Instituto Nazionale di Geophysica.

Wookey, J., Stackhouse, S., Kendall, J. M., Brodholt, J., & Price, G. D. (2005). Efficacy of the post-perovskite phase as an explanation for lowermost-mantle seismic properties. *Nature*, *438*, 1004–1007. https://doi.org/10.1038/nature04345

Wysession, M. E., Lay, T., Revenaugh, J., Williams, Q., Garnero, E. J., Jeanloz, R., & Kellogg, L. H. (1998). The D" discontinuity and its implications. In M. Gurnis, M. E. Wysession, E. Knittle, & B. A. Buffett (Eds.), *The core-mantle boundary region, Geodynamical Series* (Vol. 28, pp. 273–297). American Geophysical Union. https://doi.org/10.1029/gd028p0273